Morphology and membrane properties of neurones in the cat ventrobasal thalamus *in vitro*

Jonathan P. Turner, Caroline M. Anderson, Stephen R. Williams
and Vincenzo Crunelli*

Physiology Unit, School of Molecular and Medical Biosciences, University of Wales Cardiff, Museum Avenue, Cardiff CF1 1SS, UK

1. The morphological ($n = 66$) and electrophysiological ($n = 41$) properties of eighty-six thalamocortical (TC) neurones and those of one interneurone in the cat ventrobasal (VB) thalamus were examined using an *in vitro* slice preparation. The resting membrane potential for thirty-seven TC neurones was $-61 \cdot 9 \pm 0 \cdot 7$ mV, with thirteen neurones exhibiting delta oscillation with and without DC injection.

2. The voltage–current relationships of TC neurones were highly non-linear, with a mean peak input resistance of $254 \cdot 4$ MΩ and a mean steady-state input resistance of $80 \cdot 6$ MΩ between -60 and -75 mV. At potentials more positive than -60 mV, outward rectification led to a mean steady-state input resistance of $13 \cdot 3$ MΩ. At potentials more negative than -75 mV, there was inward rectification, consisting of a fast component leading to a mean peak input resistance of $14 \cdot 5$ MΩ, and a slow time-dependent component leading to a mean steady-state input resistance of $10 \cdot 6$ MΩ.

3. Above -60 mV, three types of firing were exhibited by TC neurones. The first was an accelerating pattern associated with little spike broadening and a late component in the spike after-hyperpolarization. The second was an accommodating or intermittent pattern associated with spike broadening, while the third was a burst-suppressed pattern of firing also associated with spike broadening, but with broader spikes of a smaller amplitude. All TC neurones evoked high frequency (310–520 Hz) burst firing mediated by a low threshold Ca^{2+} potential.

4. Morphologically TC neurones were divided into two groups: Type I ($n = 31$ neurones) which had larger soma, dendritic arbors that occupied more space, thicker primary dendrites and daughter dendrites that followed a more direct course than Type II ($n = 35$). The only electrophysiological differences were that Type I neurones ($n = 16$) had smaller peak input and outward rectification resistance and spike after-hyperpolarization, but greater peak inward rectification resistance, and exhibited delta oscillation less often than Type II ($n = 13$).

5. The morphologically identified interneurone exhibited no outward rectification, only moderate inward rectification, and no high frequency firing associated with the offset of negative current steps below -55 mV. This interneurone had a regular accommodating firing pattern, but the spike after-hyperpolarization had a late component, unlike the accommodating firing in TC neurones.

6. Therefore, the differentiation of TC neuronal types in the cat VB thalamus based on their morphology was reflected by differences in peak input resistance, outward rectification and spike after-hyperpolarization, which could be accounted for by their difference in soma size. More importantly, the firing pattern of the majority of TC neurones in the cat VB thalamus were different from those of TC neurones in other sensory thalamic nuclei.

7. Thalamocortical neurones in the cat VB thalamus were also clearly distinguishable from the interneurone based on the presence of their prominent outward rectification, peak inward rectification and robust low threshold Ca^{2+} potentials.

* To whom correspondence should be addressed.

The ventrobasal (VB) thalamus, the primary somatosensory region of the thalamus, consists of the ventral posterior medial (VPM) and ventral posterior lateral (VPL) nuclei, and contains small and large thalamocortical (TC) neurones projecting to layers 1 and 2 and layers 4 and 5 of the somatosensory cortex, respectively (Penny, Itoh & Diamond, 1982; Rausell & Avendaño, 1985), and local circuit interneurones (Spreafico, Schmechel, Ellis & Rustioni, 1983a; Yen, Conley & Jones, 1985). A large number of *in vivo* and *in vitro* studies has also investigated the electrical behaviour of VB neurones with respect to its role in somatosensory processing (Salt, 1986; Gottshalt, Vahle-Hinz & Hicks, 1989), sleep rhythms (Steriade, Jones & Llinás, 1990) and absence epilepsy (Prince & Farrell, 1969; Huguenard & Prince, 1994), and, in particular, this nuclear complex is one of the main thalamic sites to record activity associated with delta waves during slow wave sleep (Steriade & Contreras, 1995) and with the spike and wave discharge of absence epilepsy (Avoli & Gloor, 1982; Vergnes, Marescaux & Depaulis, 1990). However, no systematic analysis of the subthreshold membrane properties and firing patterns of TC neurones and interneurones in the VB has been carried out so far, and, in view of recent findings, it would be inappropriate to deduce this information by a simple process of analogy from similar neuronal types in other thalamic nuclear groups. In fact, although the original electrophysiological studies on the membrane properties of TC neurones had indicated a large degree of similarity across nuclei and species (Jahnsen & Llinás, 1984a,b; Deschênes, Paradis, Roy & Steriade, 1984; Jones, 1985), clear differences have also been highlighted by recent investigations. In particular, intracellular recording *in vivo* has indicated that there are differences between intralaminar and sensory thalamic nuclear groups (Steriade, Curró-Dossi & Contreras, 1993), and the inward rectifying current I_h has been shown to be absent from TC neurones of the dorsal medial geniculate nucleus (Hu, 1995), unlike the ventral medial geniculate nucleus and other thalamic nuclei (McCormick & Pape, 1990; Hu, 1995). In addition, within each thalamic nucleus, electrophysiological analysis using intracellular current clamp recordings *in vitro* has shown that TC neurones and interneurones are distinguishable on the basis of their membrane properties (Jahnsen & Llinás, 1984a; Deschênes *et al.* 1984; Pape & McCormick, 1995; Williams, Turner, Anderson & Crunelli, 1996), although in the dorsal lateral geniculate nucleus (dLGN) this distinction between TC neurones and interneurones is less clear under voltage clamp conditions, since it merely reflects the differences in the size and/or the voltage dependence of some of their intrinsic ionic conductances (Pape, Budde, Mager & Kisvarday, 1994).

The aim of the present study, therefore, was to examine the membrane and firing properties of neurones in the cat VB thalamus and, by ascertaining their morphology, to compare these properties for small and large TC neurones. The findings presented here, and in the accompanying

papers (Williams, Tóth, Turner, Hughes & Crunelli, 1997a; Williams, Turner, Hughes & Crunelli, 1997b), clearly indicate the presence of important differences and similarities with other thalamic nuclei and between large and small TC neurones within the VB. Some of these results have been published in preliminary form (Turner, Anderson & Crunelli, 1994).

METHODS

Preparation of cat VB thalamic slices

Young adult male and female cats (1–1·5 kg) were deeply anaesthetized with a mixture of O_2 and NO_2 (2:1) and 1% halothane. The top of the skull was exposed, a wide craniotomy performed and the meninges were removed. The animals were killed by a coronal cut at the level of the inferior colliculus, and, following transection of the optic tracts, the brain was removed and submerged in ice-cold (1–4 °C) oxygenated (95% O_2–5% CO_2) modified Krebs medium containing (mM): KCl, 5; KH_2PO_4, 1·25; $MgSO_4$, 5; $CaCl_2$, 1; $NaHCO_3$, 16; glucose, 10; sucrose, 250. The brain was bisected along the mid-line and each half was trimmed dorsally, laterally and rostrally to generate a block of tissue containing the whole thalamus. Each block was then affixed, ventral surface uppermost, to the cutting stage of a Vibroslice (Campden Instruments) with cyanoacrylate adhesive and trimmed until the ventral surface of the VB was visible, at the level of the anterior commisure (see plate 148 of Berman & Jones, 1982). Horizontal sections 500 μm thick were then cut and slices of VB thalamus prepared by excising the more lateral regions of the main thalamic field corresponding to the VPL and VPM thalamic nuclei plus the adjacent nucleus reticularis thalami and internal capsule (see plates 144–148 of Berman & Jones, 1982; see also pp. 292–293 of Spreafico, Whitsel, Rustioni & McKenna, 1983b). The preparation of slices was stopped once the ventral surface of the dLGN was reached (see plate 143 of Berman & Jones, 1982), as the presence of the VB thalamus was no longer certain. These slices were then placed in a storage chamber containing a continuously oxygenated (95% O_2–5% CO_2) Krebs medium, in which 134 mM NaCl replaced the sucrose, and maintained at room temperature (20–22 °C).

Recording procedures

Slices were left in the storage chamber for at least 1 h before being transferred to a recording chamber where they were perfused with a continuously oxygenated (95% O_2–5% CO_2) medium of similar composition, but with 1 mM $MgSO_4$ plus 2 mM $CaCl_2$ replacing the 5 mM $MgSO_4$ plus 1 mM $CaCl_2$, respectively. This medium also contained the excitatory amino acid antagonists D,L-2-amino-5-phosphonovaleric acid (APV, 100 μM), 6-cyano-7-nitroquinoxaline-2,3-dione (CNQX, 20 μM), 1-(4-aminophenyl)-4-methyl-7,8-methylenedioxy-5H-2,3-benzodiazepine (GYKI 52466, 100 μM) and (5R,10S)-(+)-5-methyl-10,11-dihydro-5H-dibenzo[a,d]-cyclohepten-5,10-imine hydrogen malate (MK 801, 10 μM), and the inhibitory amino acid antagonists bicuculline methiodide (50 μM) and 3-aminopropyl-(diethoxymethyl)-phosphonic acid (CGP 35348, 500 μM) so that synaptic transmission mediated by ionotropic L-glutamate, $GABA_A$ and $GABA_B$ receptors would not influence the properties of recorded neurones. Slices were maintained at a temperature of 35 ± 1 °C, and left for a further 1 h before recording commenced.

In order to obtain full voltage–current plots and firing patterns using the current clamp technique, thin-walled glass micro-

electrodes (GC 120TF; Clark Electromedical Instruments) filled with 1 M potassium acetate (30–60 MΩ) were used. Biocytin (2%) was included in the intracellular recording solution, so that impaled neurones could be subsequently identified. Preliminary intracellular recordings made with standard walled glass (GC 120F, Clark Electromedical Instruments) filled with 1 M potassium acetate (70–100 MΩ) were excluded on the grounds that the pronounced inward and outward rectification of the recorded VB TC neurones may, in part, have been the result of electrode artifacts in some cases. Note, however, that the interneurone was recorded using a standard walled glass microelectrode. Upon amplification with the Axoclamp-2A, voltage and current records were stored on a Biologic DAT recorder and later analysed with pCLAMP software, having been digitized at 1–100 kHz via a DigiData 1200 interface.

Identification of neuronal types

The criteria for the identification of TC and interneurones were similar to those described previously for the dLGN (Crunelli, Kelly, Leresche & Pirchio, 1987a; Crunelli, Leresche & Parnavelas, 1987b; Pape & McCormick, 1995; Williams et al. 1996). Thus, the TC neurones were characterized using two features of their membrane properties. The first was a robust low threshold Ca^{2+} potential (LTCP) which could be evoked by the injection of either positive or negative current steps, when the membrane potential was held more negative than −65 mV. The second was the biphasic inward rectification of the voltage–current relationship at membrane potentials more negative than −75 mV, with a characteristic time-dependent depolarizing 'sag' of the membrane potential, and the outward rectification at membrane potentials more positive than −55 mV. The validity of this method was confirmed following the recovery of these neurones for histological analysis, since they all had morphologies similar to those identified in previous anatomical studies (Spreafico et al. 1983a; Yen et al. 1985; Nomura, Nishikawa & Yokota, 1992).

Analysis of membrane properties

The parameters of the voltage–current relationship used in this study were determined from voltage responses to current steps over the range −90 to −40 mV. In order to avoid the generation of a LTCP by positive current steps during the determination of the voltage–current relationship or the appearance of delta oscillation, the membrane potential of most neurones was depolarized by DC injection until the LTCP was no longer evoked by positive current steps. The voltage responses were then measured at their peak

deflection during, and at the apparent steady-state 10 ms before the offset of, the current steps. Once the two curves for the peak (Fig. 1, open circles) and steady-state (Fig. 1, filled circles) voltage–current relationship had been constructed, the slope resistance was measured by fitting regression lines to the regions of interest (Fig. 1). The voltage limits (Fig. 1, points 3 and 4) for the steep region of peak input resistance were determined from the points at which the peak voltage–current relationship deviated from the regression line (Fig. 1, line 1) fitted to the steep region.

Biocytin injection and anatomical procedures

The injection of biocytin into neurones was accomplished without using an ejection protocol (Williams et al. 1996). The location of each filled neurone was recorded on outline drawings of the brain slice. Two neurones per slice were routinely filled, separated by sufficient space to allow subsequent unequivocal identification of their dendritic field and appendages during morphological analysis. The histological processing was performed as described previously (Williams et al. 1996). The morphology of the stained neurones was examined using light microscopy and measurements of somal and dendritic area were made from camera lucida reconstructions made at × 1300 and × 200, respectively. Somal and dendritic areas were calculated according to the methods described by Spreafico et al. (1983a) where the area (A) is calculated from $A = \pi ab$, where a and b are the minimum and maximum radii, respectively. Dendritic field density analysis was performed by counting the number of dendritic branches every 20 μm, using the method of Sholl (1953). Illustrated TC neurone reconstructions were made at a magnification of × 625 and the interneurone reconstruction at × 1300.

Statistics and drug sources

Quantitative results are expressed in the text and figures as means ± S.E.M. or means with the range in parentheses, depending on whether the data were normally distributed or not (Kolmogorov–Smirnov test, SigmaStat). Significance was tested using either Student's t test or the paired t test, depending on the experimental design, if the data were normally distributed, or the Mann–Whitney U test if they were not. CNQX and APV were purchased from Tocris Cookson; MK 801 was from RBI and bicuculline methiodide from Sigma. CGP 35348 was a kind gift from Dr W. Froestl (Ciba-Geigy, Switzerland) and GYKI 52466 a kind gift from Dr I. Tarnawa (Institute for Drug Research, Budapest).

Figure 1. Analysis of the subthreshold membrane properties of TC neurones

A, typical voltage–current relationships of a VB TC neurone. One curve was obtained by measuring the peak voltage deflection during injection of positive and negative current steps and represents the peak voltage–current relationship (O); the other curve was obtained by measuring the voltage deflection at the apparent steady-state, 10 ms before the offset of the current steps, and represents the steady-state voltage–current relationship (●). 1 and 2, peak and steady-state input resistances, respectively. 3 and 4, upper and lower voltage limits, respectively, of the steep region of the peak voltage–current relationship. 5 and 6, peak and steady-state inward rectification resistances, respectively. 7, steady-state outward rectification resistance.
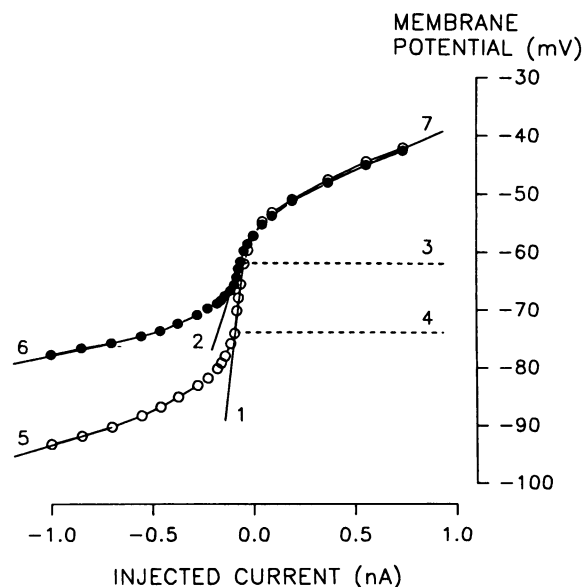
RESULTS

Intracellular recordings were obtained from a total of eighty-seven neurones in the cat VB thalamus. From these recordings, forty-one neurones were selected since only these contained all the electrophysiological data sufficient to construct the database for the TC neurones in this study. Of these forty-one neurones, twenty-nine could be visualized sufficiently well following histological processing and, without exception, these neurones were identified as being TC neurones. These twenty-nine neurones therefore represent the database of neurones for which we had complete electrophysiological and morphological data. A further thirty-seven TC neurones were sufficiently well-filled for morphological analysis to be performed, although their electrophysiological data were incomplete. Only for one recovered neurone with properties similar to VB interneurones was the complete set of electrophysiological data available. The locations of all the recorded neurones were within the boundaries of the VB thalamus (Fig. 2). No attempt was made to distinguish the shell (nociceptive and wide dynamic range units) and core (low threshold mechanoreceptive) regions, since a previous study had indicated no difference in the morphology of the neuronal types found in these regions (Spreafico *et al.* 1983*a*; Yen *et al.* 1985; Nomura *et al.* 1992).
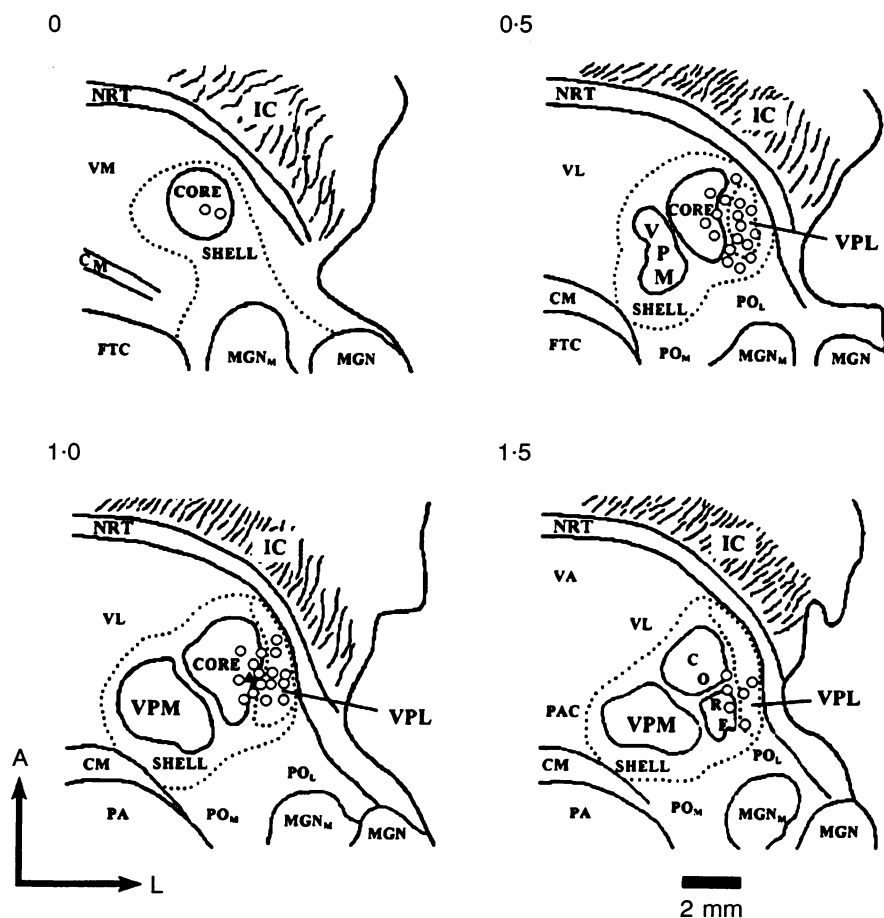

Figure 2. Location, in the cat VB thalamus, of the morphologically identified neurones with complete set of electrophysiological data

Diagramatic representations of the distinguishable territories in the cat ventral thalamus (see Berman & Jones, 1982; Spreafico *et al.* 1983*b*) illustrate the position of the forty-one TC neurones (O) and the one interneurone (▲) for which a complete set of electrophysiological data was available. Values above each drawing are the levels (in mm) at which sections were taken during the preparation of the brain slices and correspond to those of Spreafico *et al.* (1983*b*). Neurones were recorded from both core and shell regions, and the VPL nucleus, which make up the central and lateral part of the VB thalamus, respectively. Abbreviations: CM, centre median nucleus; FTC, central tegmental field; IC, internal capsule; MGN, medial geniculate nucleus; MGN_M, medial geniculate nucleus medial magnocellular region; NRT, nucleus reticularis thalami; PA, pretectal area; PAC, paracentral nucleus; PO_M, medial posterior complex; PO_L, lateral posterior complex; VA, ventral anterior nucleus; VL, ventral lateral nucleus; VM, ventral medial nucleus; VPL, ventral posteriolateral nucleus; VPM, ventral posteriomedial nucleus. A, anterior; L, lateral.
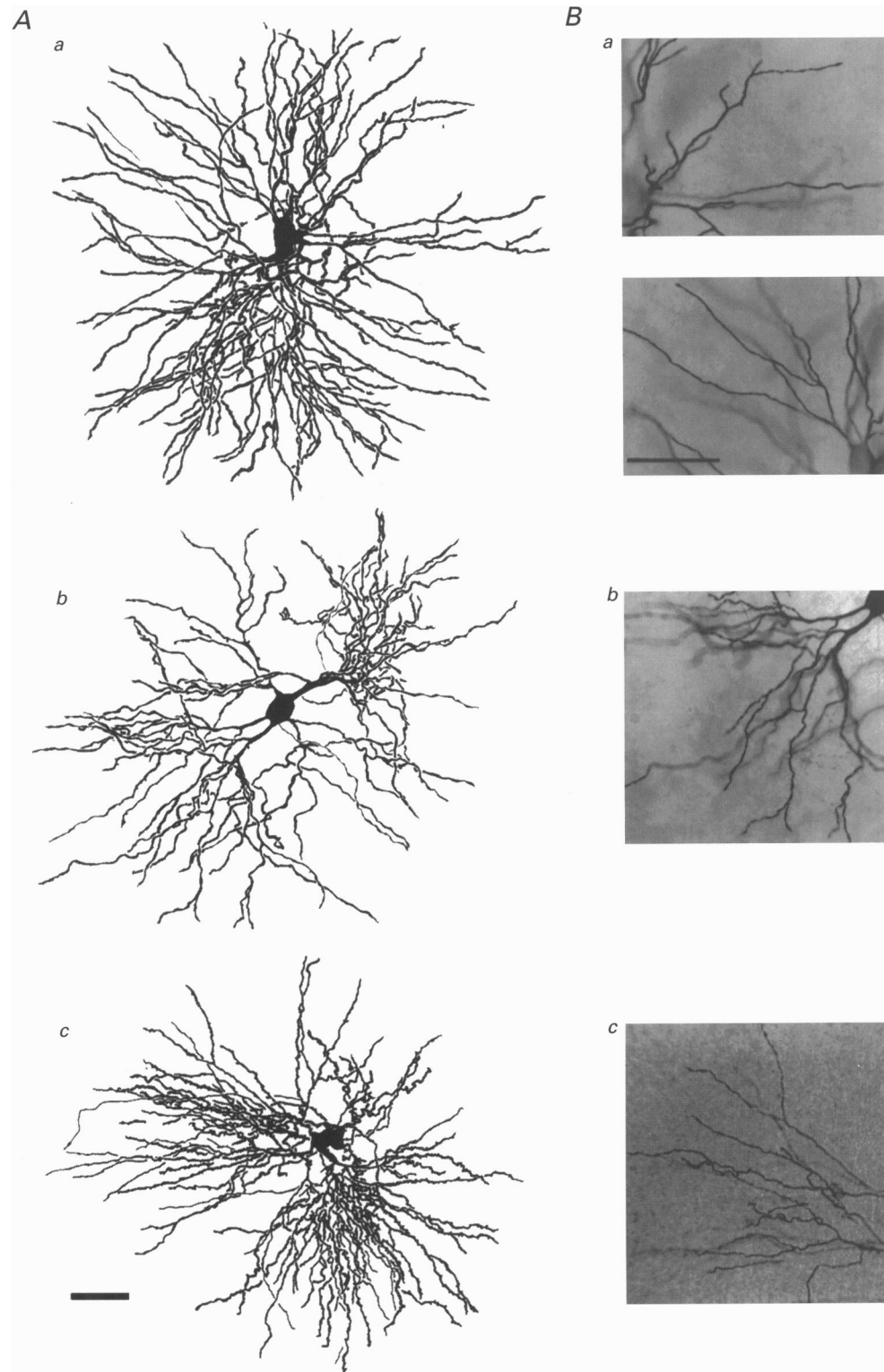
Figure 3. Morphological classification of TC neurones in the cat VB thalamus

A, camera lucida reconstructions of biocytin-injected TC neurones classified as Type I (*a*), Type II a (*b*) and Type II b (*c*). The calibration bar (50 μm) in *Ac* also applies to *Aa* and *b*. *Ba*, photomicrographs of the dendritic field to illustrate the higher order branching to the periphery (upper panel) and the direct course taken by the dendrites (lower panel) of the Type I neurone in *Aa*. *Bb*, photomicrograph of the lower left quadrant of the dendritic field of the Type II a neurone in *Ab* illustrating the tortuous course of distal dendrites with multiple bifurcations proximal to the soma. *Bc*, photomicrograph showing the course and structure of the dendrites of the Type II b neurone in *Ac*. The calibration bar (50 μm) in *Bb* applies also to *Ba* and *c*.

Table 1. Morphological parameters of TC neurones from the cat VB thalamus

	Soma area (μm^2)	Dendritic field area (mm^2)	Primary dendrite parameters		
			Number	Diameter (μm)	Length (μm)
Type I ($n = 31$)	554 (259–1090)	0·147 ± 0·007 (0·081–0·228)	6·3 (4–11)	4·5 (3·1–7·9)	15·7 ± 0·7 (7·5–25·3)
Type II ($n = 35$)	378 ± 16^d (210–598)	0·101 ± 0·004^d (0·065–0·174)	5·8 (3–9)	3·1^d (1·8–5·0)	17·1 (9·4–36·7)
Type IIa ($n = 7$)	395^a (261–592)	0·095 ± 0·008^c (0·068–0·121)	5·1^a (4–6)	3·0 ± 0·4^b (1·8–5·0)	22·7 ± 3·2^a (14·5–36·7)
Type IIb ($n = 28$)	374 ± 18^d (210–598)	0·102 ± 0·005^d (0·065–0·174)	6·0 (3–9)	3·1 ± 0·2^d (1·8–4·8)	15·6 ± 0·9^e (9·4–29·3)

Values expressed as means only indicate that the data were not normally distributed. $^aP < 0.05$, $^bP < 0.005$, $^cP = 0.001$, $^dP < 0.001$ compared with Type I. $^eP = 0.05$ compared with Type IIa (Mann–Whitney U test).

The classification of neurones in the cat VB thalamus

Three types of neurone were identified qualitatively in this study using criteria developed from previous descriptions of their dendritic morphology (Spreafico *et al.* 1983*a*; Yen *et al.* 1985): two classes of TC neurones, and a local circuit interneurone. The TC neurones were divided into two groups since the dendritic fields of Type I ($n = 31$), compared with those of Type II ($n = 35$), were typically less spatially compact, had a less tortuous course, the terminal dendritic branch points occurred further from the soma, and the diameter of the primary dendrites was greater, than for Type II ($n = 35$). No other primary dendritic characteristics were used, including the previously described 'tufting' and 'bifurcating' patterns of primary dendritic division (Yen *et al.* 1985), since tufting was rarely observed. The interneurone had a small round soma with a luxuriant and extensive dendritic arborization, as described by Spreafico *et al.* (1983*a*).

The morphology of TC neurones

Somatic and primary dendritic features of TC neurones. The soma of Type I TC neurones were generally polygonal in shape, and occasionally were 'hairy' in appearance, while those of Type II were smaller (Table 1), more spherical and had a smooth appearance (Fig. 3*Aa* and *Ba*), as described previously (Spreafico *et al.* 1983; Yen *et al.* 1985). This second group was split into two subtypes based on the length of the proximal dendrites (Table 1): Type IIa and Type IIb. Type IIa ($n = 7$) possessed at least four large primary dendrites (Fig. 3*Ab*), usually arising from opposing quadrants, which branched profusely and matched the previous description of 'small round' neurones (Spreafico *et al.* 1983), while Type IIb ($n = 28$) had shorter primary dendrites (Table 1) which branched much less profusely
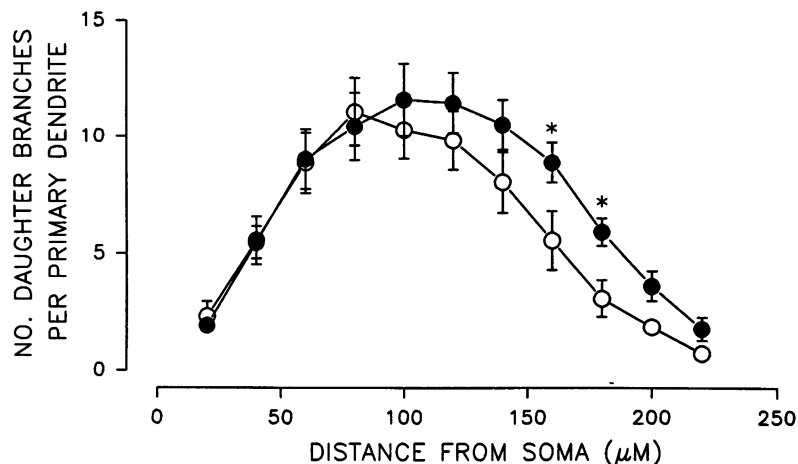

Figure 4. Dendritic branches in Type I and Type II TC neurones

The graph shows the significantly greater number of daughter dendritic branches per primary dendrite at a distance of between 160 and 180 μm from the soma for seven Type I (●) compared with six Type II (○) TC neurones. Bars represent the s.e.m. *$P < 0.05$, Student's t test.
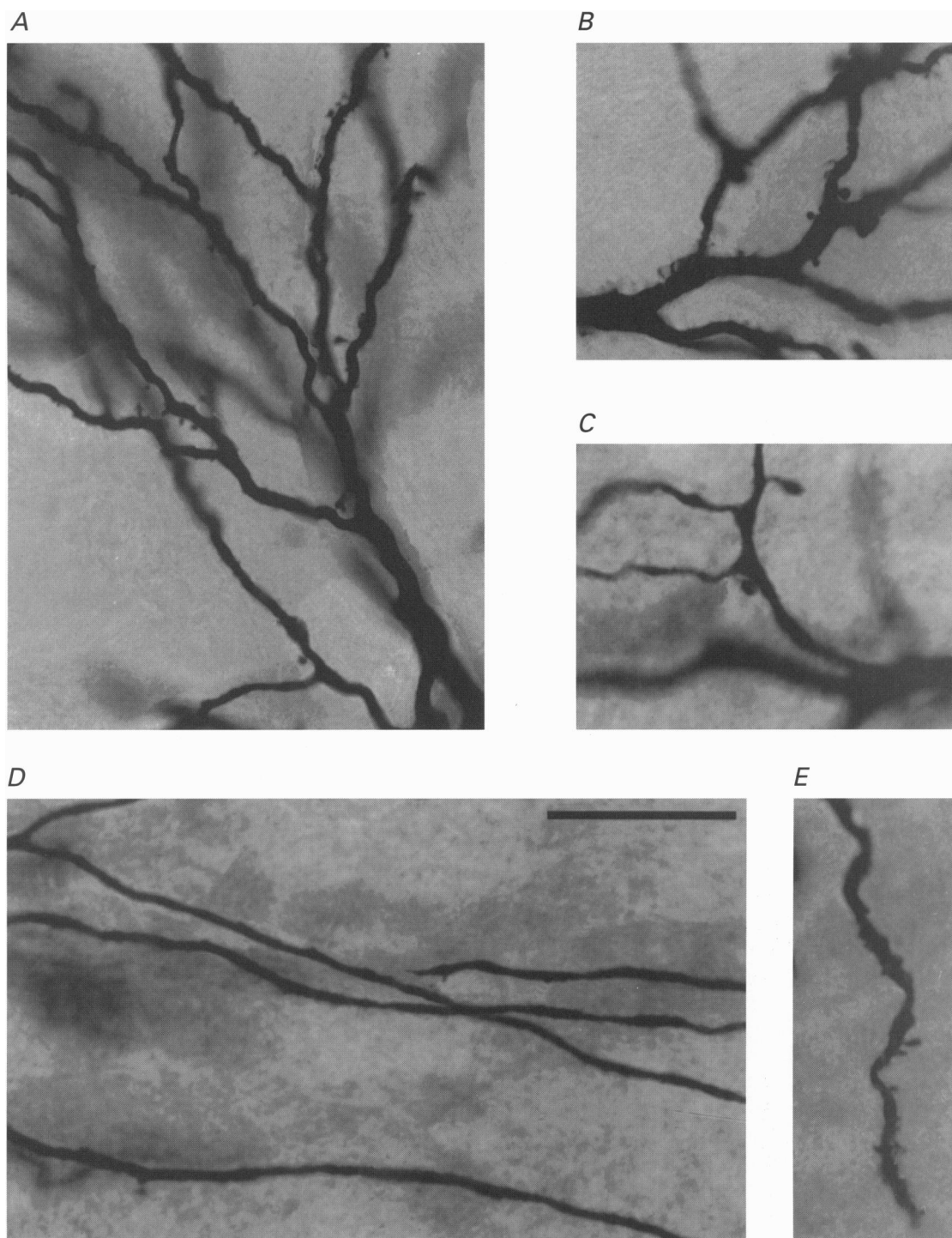
Figure 5. Dendritic appendages associated with TC neurones in the cat VB thalamus

A, photomicrograph of a Type I neurone showing appendages around primary, secondary and tertiary branch points and how their density increases towards the periphery. *B*, photomicrograph from the same Type I neurone as in *A* shows how the dendrites appear 'hairy' along their course, and the presence of small round studs close to the dendritic surface. *C*, in another Type I neurone, appendages appear at secondary and tertiary branch points on these smooth dendrites, but exhibit a more pronounced stalk. *D*, photomicrograph of a Type I TC neurone whose finer calibre dendrites follow a direct path and are devoid of appendages. *E*, photomicrograph showing appendages on the distal dendrites of a Type II neurones. The calibration bar in *D* (20 μm) applies also to *A–C* and *E*.

(Fig. 3Ac). The primary dendrites of Type I TC neurones were of similar length to Type II b but shorter than Type II a, and of larger diameter than both Type II subtypes. The secondary dendrites of Type I TC neurones showed little change in calibre compared with those of Type II, which were finer than their primaries (Table 1).

Distal dendritic features of TC neurones. The dendritic fields of Type I TC neurones were larger than that of Type II (Table 1), and the distal dendritric morphology of

Type I neurones (Fig. 3A) was characterized by being less spatially compact with dendritic calibre being maintained, following bifurcation, over a larger part of the dendritic field compared with that of Type II. In addition, the terminal branch point of Type I TC neurones occurred more distally than Type II, so that the distal dendrites made up a smaller proportion of total dendritic length, and so Type I neurones had a larger number of dendritic branches per dendritic arbor at 160–180 μm from the soma (Fig. 4).
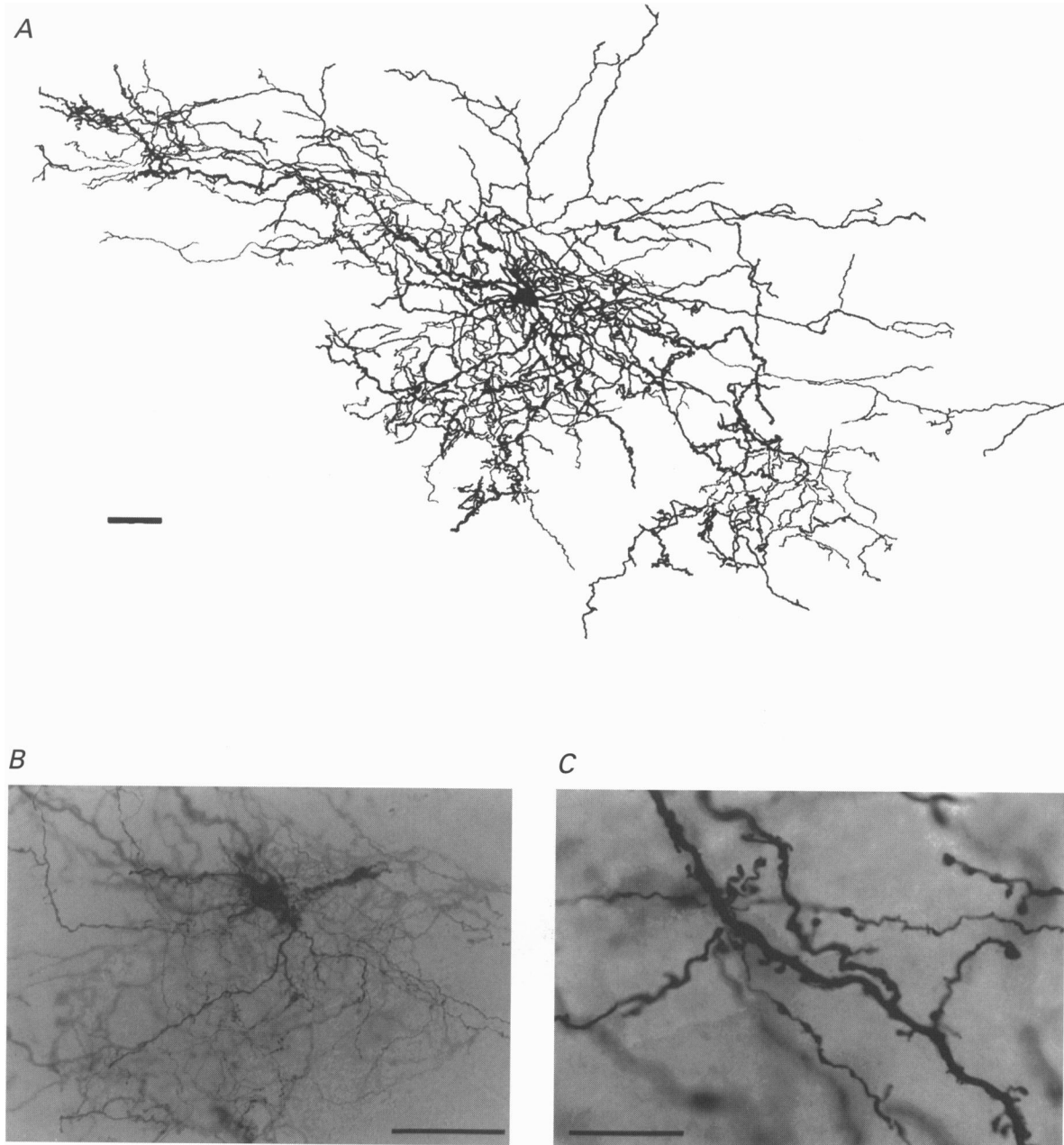

Figure 6. Morphology of an interneurone from the cat VB thalamus
A, camera lucida reconstruction showing the full extent of the dendritic/axonal arborization of a VB interneurone within the 500 μm thick slice. Calibration bar, 100 μm. *B*, photomicrograph showing the lack of large diameter dendrites and the soma surrounded by an abundance of fine, tortuous appendages. Calibration bar, 50 μm. *C*, photomicrograph illustrating the profusion of short stud-like protrusions along the dendritic length and the varicosed nature of the axon. Calibration bar, 20 μm.

Table 2. Summary of the subthreshold electrophysiological properties of TC neurones from the cat VB thalamus

		Total ($n = 41$)	−Osc ($n = 28$)	+Osc ($n = 13$)	Type I ($n = 16$)	Type II ($n = 13$)
No. oscillations		13 (31·7%)			3 (18·8%)	5 (38·5%)
Resting V_m	(mV)	−61·9 ± 0·7[a] ($n = 37$)	−62·6 ± 0·8	−59·4 ± 1·3[a] ($n = 9$)	−63·2 ± 1·2[a] ($n = 14$)	−61·2 ± 1·4[a] ($n = 11$)
AP threshold	(mV)	−42·4 ± 0·4	−42·6 ± 0·6	−41·9 ± 0·6	−43·2 ± 0·6	−42·1 ± 0·8
Peak R_{in}	(MΩ)	254·4[b] (48·9–995·3) ($n = 40$)	188·7[b] (48·9–511·6) ($n = 27$)	390·9[c] (126·2–995·3)	134·1[b] (48·9–269·8) ($n = 15$)	372·4[c] (111·2–995·3)
Steady-state R_{in}	(MΩ)	80·6[b] (31·0–238·7) ($n = 40$)	75·2[b] (31·0–238·7) ($n = 27$)	91·9 (40·4–193·0)	66·5[b] (31·0–139·5) ($n = 15$)	105·4 (35·3–238·7)
Upper R_{in} limit	(mV)	−59·8 ± 0·4	−60·3 ± 0·6	−58·6 ± 0·7	−59·8 ± 0·7	−59·4 ± 0·6
Lower R_{in} limit	(mV)	−75·5 ± 1·3	−75·4 ± 1·8	−75·5 ± 0·9	−75·1 ± 1·1	−74·5 ± 0·9
Peak IR slope resistance	(MΩ)	14·5 (8·2–37·8)	5·2 (8·2–37·8)	13·1 (10·3–18·0)	17·5 (8·2–37·8)	12·5[c] (8·8–17·9)
Steady-state IR slope resistance	(MΩ)	10·6 (4·1–24·2)	9·6 (4·1–24·2)	12·7[c] (7·4–23·0)	9·9 (4·1–19·7)	11·7 (4·4–24·2)
IR regression slope[d]		—	0·40 ± 0·03 ($n = 28$)	—	0·41 ± 0·04 ($n = 13$)	0·35 ± 0·06 ($n = 8$)
Steady-state OR slope resistance	(MΩ)	13·3 ± 1·11	12·2 ± 0·9	15·8 ± 2·9	10·5 ± 1·2	16·2 ± 2·4[c]

Values expressed as means only (range in parentheses) indicate that the data were not normally distributed. Osc, oscillation. V_m, membrane potential; AP, action potential; R_{in}, input resistance; IR and OR, inward and outward rectification, respectively. [a] Some neurones exhibited delta oscillation in the absence of injected DC. [b] One neurone exhibited bistability in the voltage–current relationship. [c] $P < 0.05$ (student's t test or Mann–Whitney U test). [d] The regression slopes for the relationship between the amplitude of the depolarizing sag *versus* the peak voltage response during negative current steps.

The dendritic paths of Type I TC neurones varied from those which were tortuous yet quite direct (Fig. 3*Aa* and *b*), to a completely straight course (Fig. 5*D*), coincident with a finer dendritic calibre and smooth appearance. In contrast, Type II were typified by a sinuous path with tortuous twists, providing the appearance of a 'knot' of dendrites (Fig. 3*Ba*, *Bb*, *Ca* and *Cb*) as daughters emerged at oblique angles.

For both Type I and II TC neurones with tortuous dendritic paths, stud-like appendages were observed singly or in clusters, proximal to primary, secondary or tertiary branch points (Fig. 5*A–C* and *E*). Those Type I TC neurones with tortuous dendritic paths also had short hair-like protrusions, which increased in density towards the periphery of the dendritic field, and which, in a few cases, were also present on the soma, lending these neurones their hairy appearance (Fig. 3*Aa*). In contrast, Type I TC neurones with smooth straight dendrites had no appendages at all (Fig. 5*D*).

The morphology of an interneurone

The putative interneurones had a small round soma (area, 234·8 μm^2), and four identifiable principle dendrites (Fig. 6). At each primary dendritic branch point, there was a profusion of secondary dendritic processes, forming an extensive dendritic field (area, 0·254 mm^2), whose total volume was probably truncated by the brain slicing procedure. Along the length of each dendrite there were many stud-like protrusions with thin thread-like appendages arising at regular intervals. These appendages bifurcated repeatedly forming a dense network (Fig. 6*B*), with each fibre exhibiting varicosities along their entire length (Fig. 6*C*).

The membrane properties of TC neurones

Resting membrane potential and delta oscillation. A mean stable resting membrane potential of −61·9 ± 0·7 mV was measured for thirty-seven of the forty-one TC neurones studied (Table 2). The four remaining TC neurones had non-stable membrane potentials in the absence of injected DC, owing to the presence of delta (or pacemaker) oscillation (frequency range, 1–4 Hz), as demonstrated in other thalamic nuclei both *in vitro* and *in vivo* (McCormick & Pape, 1990; Leresche, Lightowler, Soltesz, Jassik-Gerschenfeld & Crunelli, 1991; Nuñez, Amzica & Steriade 1992). Nine of the thirty-seven TC neurones with stable resting membrane potentials also exhibited delta oscillation when either positive or negative DC was injected (Fig. 7*A*), so that 32%

of all TC neurones exhibited delta oscillation (Table 2). In addition, TC neurones exhibiting delta oscillation had significantly greater mean peak input resistance than those that did not show oscillation (Table 2), suggesting that the TC neurones with larger peak input resistances are more likely to exhibit delta oscillation.

Voltage–current relationship. The voltage–current relationship (determined at a membrane potential of −57·4 ± 0·4 mV) was highly non-linear for all TC neurones (Fig. 8), and characterized by a steep region with the highest peak input resistance between −59·8 ± 0·4 and −75·4 ± 1·3 mV (Table 2). The mean peak input resistance over this region was 254·3 MΩ, (48·9–995·3 MΩ) and the

distribution of these values was skewed towards the higher values (Fig. 7B). These peak input resistance values were not correlated to resting membrane potential ($r = 0·14$, $P > 0·1$, $n = 37$), suggesting that the subthreshold conductances responsible for the peak input resistance are not involved in determining resting membrane potential. The examination of voltage responses to negative current steps in this membrane potential range has been used to establish the passive membrane properties of TC neurones (Bloomfield, Hamos & Sherman, 1987; Crunelli *et al.* 1987*b*; Williams *et al.* 1996). In this membrane potential range there was also a clear depolarizing sag of the voltage response to negative current steps for all TC neurones, even for those with lower input resistance (as the one shown in
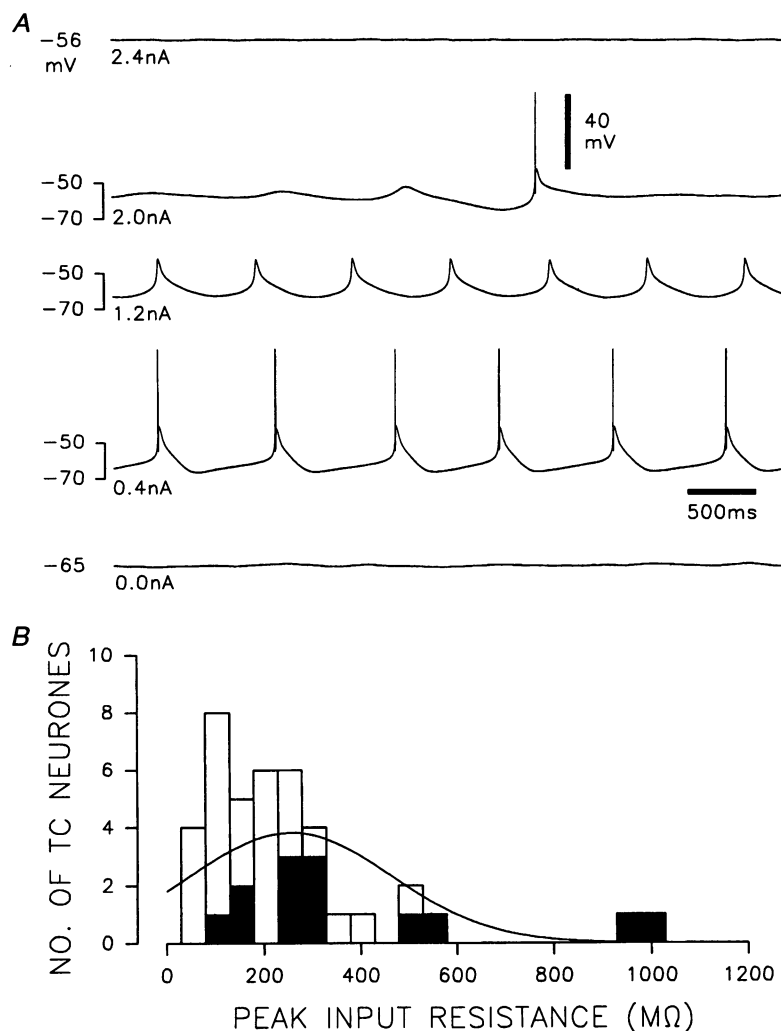

Figure 7. Delta oscillation and input resistance of TC neurones from the cat VB thalamus

A, voltage records illustrating the nature of the delta oscillation, and the voltage range over which this activity occurs. The uppermost and lowermost records are at the stable membrane potentials below and above which, respectively, changes in injected DC elicit the types of voltage fluctuations illustrated by the intermediate traces. The second trace down illustrates how membrane potential moves in and out of the oscillation envelope at its uppermost extreme. The frequency of the delta oscillations in the third and fourth traces down are 1·4 and 1·2 Hz, respectively. The injected DC values are below, and the voltage values to the left of, each trace. The amplitude of the action potentials has been truncated for clarity. *B*, distribution histogram for the peak input resistance values with fitted Gaussian curve. Filled and open columns indicate neurones capable or incapable of producing delta oscillations, respectively.

Fig. 8*Aa*), so that the mean steady-state input resistance was 80·6 MΩ (*n* = 40) (Table 2). Therefore, none of these neurones had membrane properties that could be considered passive in the −60 to −75 mV range, and analysis of the electrotonic structure of these TC neurones was not performed. For TC neurones with higher input resistance, voltage responses in this range were characterized either by non-monoexponential change of the membrane potential (Fig. 8*Ab*, inset) or by a multiphasic response (Fig. 8*Ac*, inset). Thus, there was a more dynamic voltage response to injected current, characterized by the peak of the voltage response, and hence the peak input resistance, being time dependent over a period of several hundred milliseconds (Fig. 8*Ac* and *d*). In addition, this behaviour resulted in an increased non-linearity in the voltage–current relationship for TC neurones of the cat VB thalamus (Fig. 8*Ba–d*), in comparison to those previously reported for other thalamic nuclei (Bloomfield *et al.* 1987; Crunelli *et al.* 1987*a,b*; Williams *et al.* 1996), such that one neurone exhibited apparent membrane bistability (Fig. 8*Bd*), where two voltage responses of differing amplitude could be evoked by a current step of the same amplitude (Fig. 8*Ad*). A detailed investigation of these phenomena is presented in the accompanying paper (Williams *et al.* 1997*a*).

Inward rectification. The inward rectification consisted of two distinct phases. The initial phase occurred within the first 100–500 ms of current injection, and was characterized by a non-linear increase in the voltage response with respect to injected current (Fig. 8), so that over the rectified range below −80 mV the mean peak input resistance was 14·5 MΩ (8·2–37·8 MΩ) (Table 2). This peak inward rectification resistance was found to be inversely correlated to the peak input resistance of the steep region of the voltage–current relationship ($r = 0·387$, $P < 0·05$, $n = 40$), indicating that TC neurones with the more dynamic voltage responses in the steep region of the voltage–current relationship exhibit more peak inward rectification. Subsequent to this, there was a slow time-dependent rectification apparent as a depolarizing sag of the membrane potential between 500–2000 ms, which led to a mean steady-state input resistance of 10·6 MΩ (4·1–24·2 MΩ) (Table 2). This steady-state inward rectification resistance was not correlated to the peak input resistance ($r = 0·075$, $P > 0·1$, $n = 40$). There was, however, a positive correlation between the size of the depolarizing sag and the peak of the voltage response for each of the non-oscillating neurones ($P < 0·05–0·01$, $n = 28$) (Table 2). A detailed analysis of the properties of inward rectification in TC neurones of the cat VB thalamus is presented in the accompanying paper (Williams *et al.* 1997*b*).

Outward rectification and action potential threshold. The voltage responses to positive current steps peaked either within the first 100 ms followed by a hyperpolarizing sag of the membrane potential (Fig. 8*Ab*), or at the end of the step following a slow depolarizing ramp (Fig. 8*Ad*), or reflected a combination of the two (Fig. 8*Aa* and *c*). These responses showed a pronounced outward rectification in the voltage–current relationship, with an input resistance of 13·3 ± 1·1 MΩ. As the membrane potential approached action potential threshold, there was an increase in small amplitude voltage perturbations, indicative of the interaction of voltage-dependent conductances in the range of voltage just subthreshold. The threshold for action potential firing was −42·4 ± 0·4 mV for all forty-one TC neurones, with the individual values being positively correlated to the peak input resistance ($r = 0·324$, $P < 0·05$, $n = 41$), but not to the outward rectification resistance ($r = 0·169$, $P > 0·1$, $n = 41$), suggesting that the subthreshold conductances responsible for the peak input resistance, but not outward rectification, influence firing threshold.

LTCP and associated burst firing. Characteristically, LTCPs were evoked in all forty-one TC neurones at the offset of negative current steps during the determination of the voltage–current relationships. The mean maximum number of action potentials evoked by the LTCP in each TC neurone was seven (3–12), with an interspike frequency for the first interspike interval of 414 Hz (317–507 Hz). This interspike frequency was correlated to the overall number of spikes in the burst ($r = 0·331$, $P < 0·05$, $n = 41$) (Fig. 9*Ba–d*), but not to the membrane potential prior to the offset of the current step ($r = 0·074$, $P > 0·1$, $n = 41$). In addition, the first spike in the burst was always the largest in amplitude, with the second spike the smallest (see, for example, the dramatic decrease in amplitude for the neurone in Fig. 9*Ab*) and each subsequent spike showing some recovery of spike amplitude towards that of the first (Fig. 9*Aa–d*). Note also that, while the higher input resistance of the neurone in Fig. 9*Ab* (compared with *Aa*) could have been responsible for the larger number of action potentials in the bursts, for the neurones in Fig. 9*Ac* and *d* with the much higher input resistance there was a smaller number of action potentials. The large number of action potentials and their characteristic decrease in amplitude could represent a peculiarity of the cat VB thalamus compared with other thalamic nuclei.

Firing patterns. The pattern of action potential discharge evoked in TC neurones of the cat VB thalamus by positive current steps from a membrane potential of −60 mV was highly variable, but could be classified into three categories (Fig. 10*A* and *B*). The first type, accelerating, was characterized by a regular accelerating firing pattern ($n = 4$) at a relatively low frequency between 20–70 Hz (Fig. 10*A*). The second type was characterized by a marked decrease in spike frequency ($n = 24$), with firing either being accommodating (i.e. regular firing at an initial frequency of 90–140 Hz, then decreasing to 20–60 Hz), or being intermittent (i.e. an initial period of firing at a frequency of 80–200 Hz, followed by irregular periods of firing with a frequency up to 80 Hz). The third group, burst-suppressed firing, was characterized by an initial burst of action potentials at 60–270 Hz, associated with an attenuation of spike amplitude, followed by a period of quiescence or
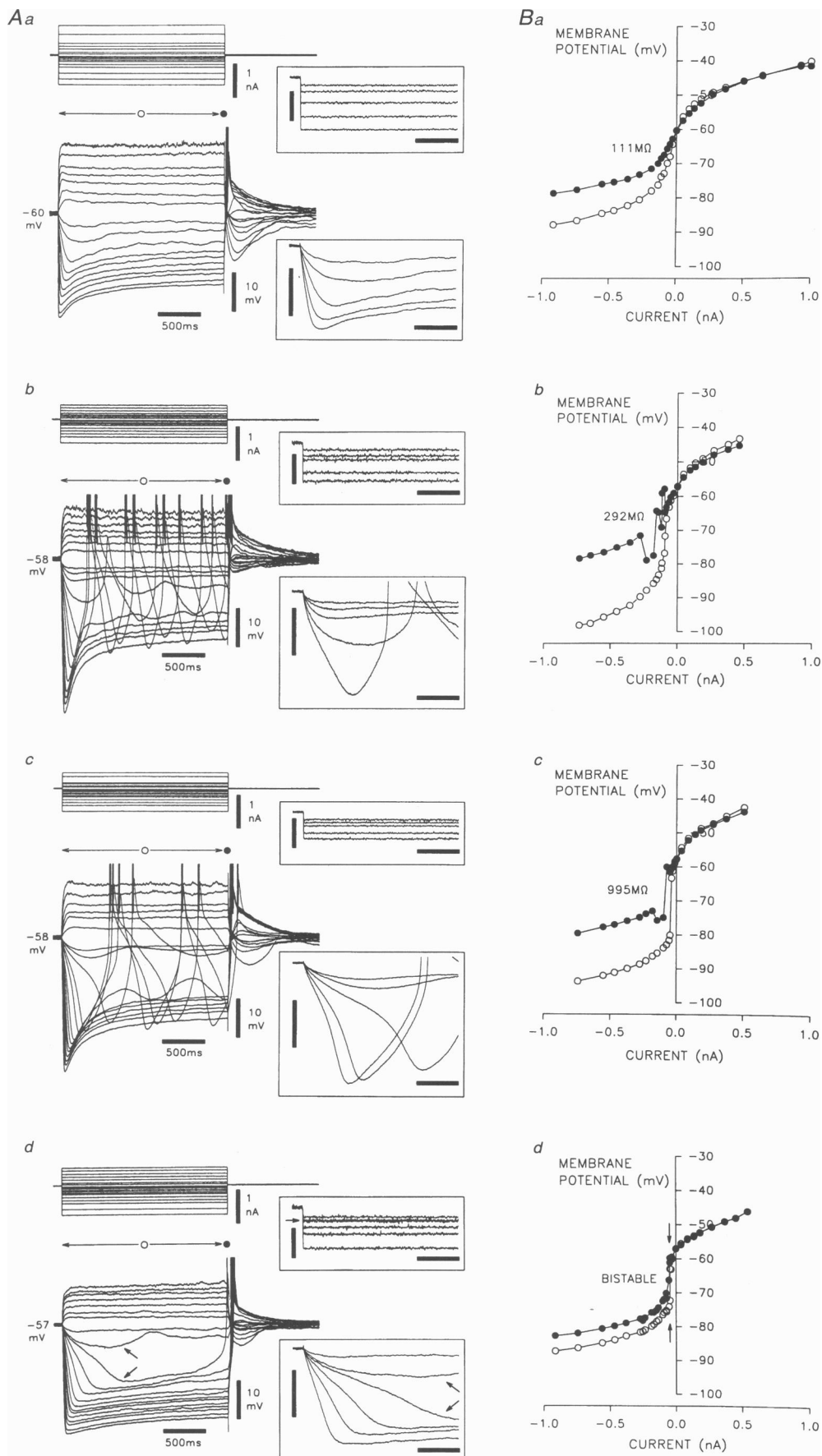
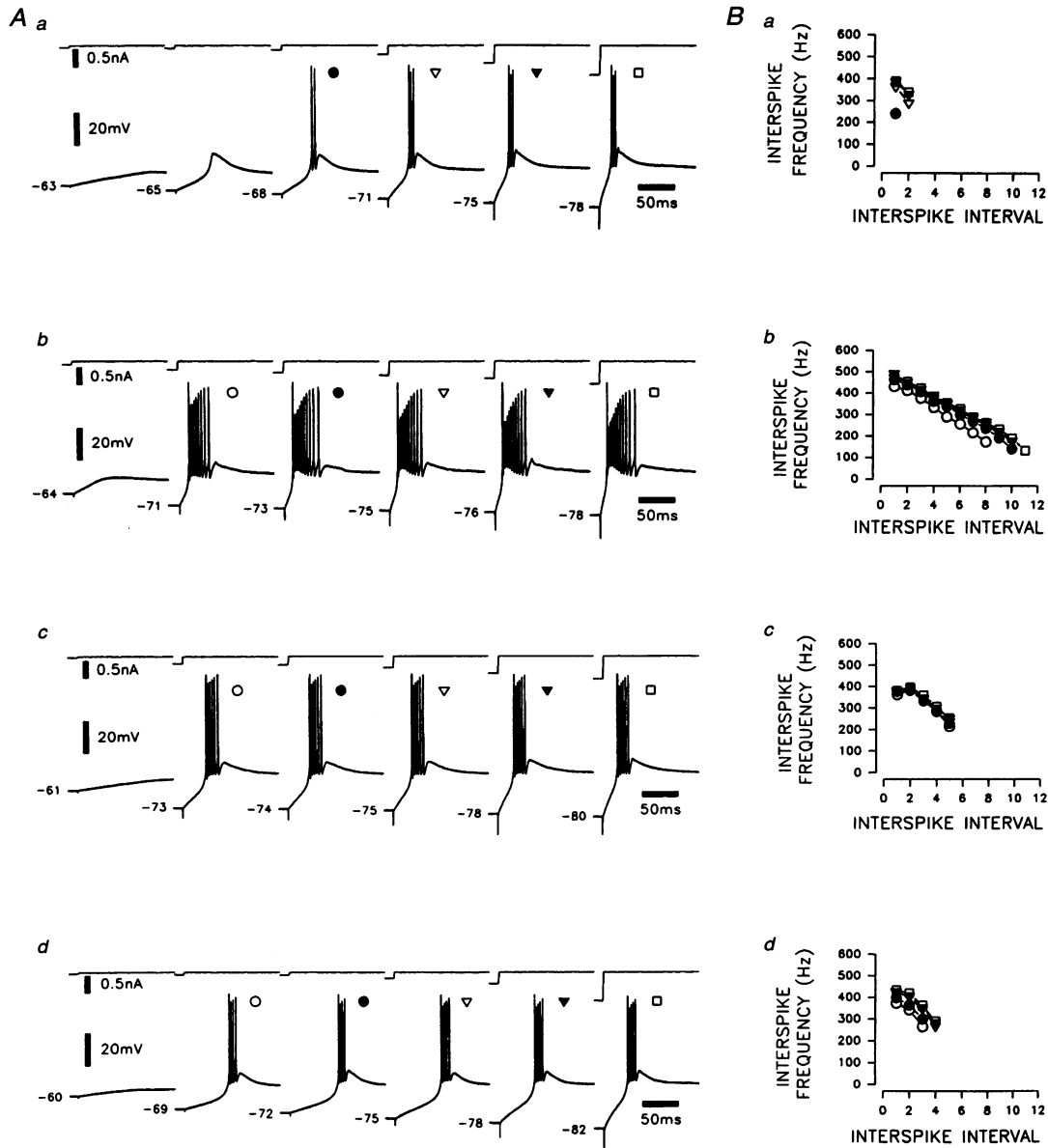Figure 8. For legend see facing page.

Figure 9. LTCP and burst firing properties of TC neurones from the cat VB thalamus

Aa–d, voltage traces illustrating the LTCPs and the associated burst of action potentials generated at the offset of the 2 s negative current step from the same TC neurones as in Fig. 9*Aa–d*, respectively. In each case, the first spike in the burst is the largest in amplitude, with the second spike the smallest and each subsequent spike showing some recovery of spike amplitude towards that of the first. The membrane potential just prior to each current step offset is shown to the left of each trace. *Ba–d*, the graphs show the inverse relationship between LTCP-evoked action potential interspike frequency and the interspike interval for the bursts indicated by the symbols above the traces in *Aa–d*.

Figure 8. *V–I* relationships of four representative TC neurones from the cat VB thalamus

Aa–d, the overlay of voltage responses (lower traces) of four TC neurones to current steps (upper traces). The insets are an overlay of selected voltage responses (lower inset) to the low amplitude (0·01–0·10 nA) current steps (upper inset). Note that, while the TC neurone in *Aa* has voltage responses of conventional electrotonic structure, and a relatively linear relationship to the current injection (see inset), those in *Ab–d* possess a highly non-linear relationship between injected current and the amplitude and time to peak of the voltage response, particularly for the neurones illustrated in *Ac* and *d* (see insets). In *Ad*, the arrows mark the two voltage responses that could be obtained by the same current step. Calibration bars in the insets represents 1 nA, 10 mV and 200 ms. The amplitude of the action potentials has been truncated for clarity. *Ba–d*, the voltage–current relationships determined at the times indicated by the corresponding symbols in *Aa–d* (O, peak; ●, steady state). Note that in *Bb* and *c* the abrupt deviations from a smooth sigmoid voltage–current relationship measured in the steady state (apparent over the range of membrane potential between −60 and −75 mV) result from the presence of a LTCP at the time of measurement (see voltage records in *Ab* and *c*). The peak input resistance in the steep region of the voltage–current relationship is indicated in each plot.

intermittent attenuated action potentials ($n = 13$). The first action potential of the burst evoked during this type of firing was characteristically smaller in amplitude in comparison to the second action potential (Figs 10*Ab* and 11*D* inset) (Table 3). In addition, the first action potential of burst-suppressed firing had a slower rise time compared with the second, but the decay was faster. All but the accelerating type of firing were associated with marked spike broadening (Fig. 10*C*). These different firing patterns were observed in sequential recordings from the same slice.

Single action potential properties. There was a clear division between accelerating and accommodating/intermittent firing (Fig. 10), for which single action potentials could be evoked (Fig. 11*A–C*), and burst-suppressed firing, for which action potentials always occurred in bursts (Fig. 11*D*). For the accelerating and accommodating/intermittent firing patterns, action potential amplitudes were very similar, and were significantly larger than those of the

burst-suppressed firing. However, the action potentials of all firing types had similar rise times, except the first action potential of burst-suppressed firing (Table 3). In addition, the action potentials associated with accelerating firing patterns had a faster decay than those of the other types, so that the mean half-width of the action potential of the accelerating firing was smaller than that of the accommodating/intermittent firing, which in turn was smaller than that of the burst-suppressed pattern.

The after-hyperpolarizations of the action potentials for accelerating and accommodating/intermittent firing types were of similar amplitude, although those for the accelerating type had a slower time to peak and decay, owing to the presence of a late component (Fig. 11*A–C*) (Table 3). The first but not the second action potential for the burst-suppressed firing had an after-hyperpolarization that was larger in amplitude than that of the other types, but both had a time to peak comparable to that of the accommodating type.
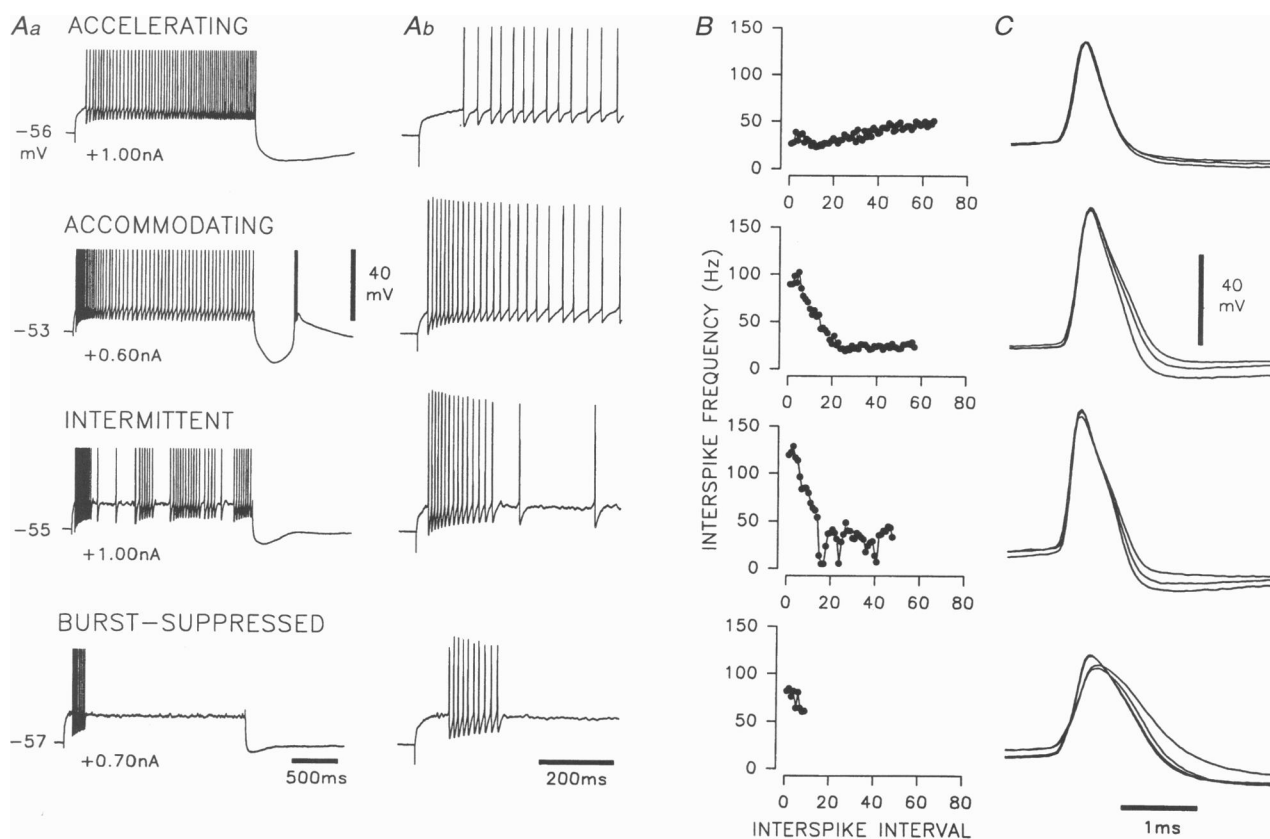

Figure 10. Firing patterns of TC neurones from the cat VB thalamus

Aa and *b*, firing patterns of TC neurones generated in response to positive current steps from membrane potentials more positive than −60 mV. Note that, unlike the burst firing evoked by the LTCP, the amplitude of the second spike is always similar to, or greater than, that of the first, and that a LTCP can be evoked at the offset of the positive current step (see trace accommodating, *Aa*). The initial membrane potential is shown to the left of each trace and the amplitude of the current step beneath each trace in *Aa*. The action potential amplitude has been truncated for clarity in *Aa*, but not in *Ab*. *B*, the relationship between interspike frequency and interspike interval number illustrates the features of these firing types (see text for details). *C*, the overlay of the first, third and tenth action potentials from the corresponding traces in *Ab*, except for the burst-suppressed type, where the first, second, third and tenth are illustrated. Note the marked increase in spike duration for all but the accelerating firing pattern.

Since burst-suppressed action potentials occurred at a frequency greater than 50 Hz, the after-hyperpolarization decay was very short.

The correlation of membrane properties with morphology

The somal area and the peak input resistance were inversely correlated for all twenty-nine TC neurones ($r = 362$, $P < 0.05$, $n = 29$), as would be predicted if the peak input resistance were a passive membrane property, but while Type I neurones showed this inverse correlation ($r = 0.585$, $P < 0.05$, $n = 16$), Type II did not ($r = 0.181$, $P > 0.1$, $n = 13$). This could be explained by the non-linear behaviour of the voltage responses in the -60 to -75 mV range over which peak input resistance was measured. Therefore, as Type II TC neurones have higher peak input resistances than Type I (Table 2) and exhibited more non-linear behaviour over this range, the measured peak input resistance probably deviates more from the passive membrane input resistance.

All differences in the subthreshold properties of the morphologically identified TC neurones were consistent with an underlying difference in the peak input resistance. Certainly, the larger outward rectification resistance for Type II TC neurones, compared with Type I (Table 2), was consistent with a higher peak input resistance, if the underlying leakage resistance was also higher. However, the reason for the smaller peak inward rectification resistance of Type II TC neurones was less clear, but in view of the later time to peak of the voltage responses of these neurones, more of the slow time-dependent inward rectification probably contributed to the peak of the voltage responses. Indeed, the steady-state inward rectification resistance for Type II TC neurones was slightly larger than that for Type I (Table 2).
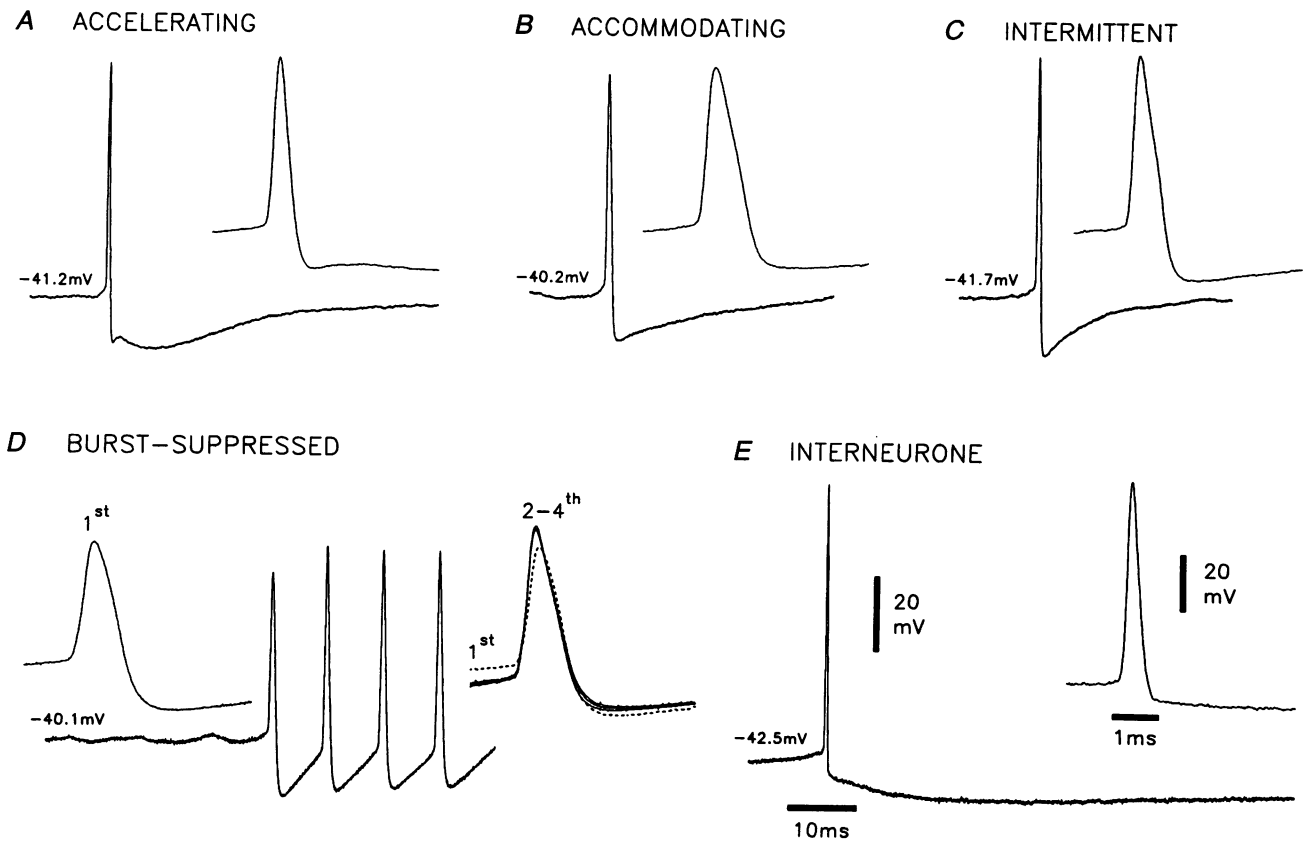

Figure 11. Types of action potential generated by TC neurones and an interneurone from the cat VB thalamus

A–D, the different types of action potential waveforms associated with the different firing patterns of TC neurones, as indicated. *E*, the action potential waveform generated from an interneurone. The insets illustrate the action potential waveforms at higher resolution. In *D*, the inset to the left of the trace illustrates the first action potential waveform in the burst, and the inset to the right an overlay of the remaining three action potential waveforms with the first superimposed as the dotted line. The mean action potential threshold is shown at the start of each record. Note the prominent biphasic after-hyperpolarization of the action potential in the interneurone and in the accelerating TC neurone firing type, in comparison to the monophasic after-hyperpolarization of the accommodating, intermittent and burst-suppressed firing types (see Table 3).
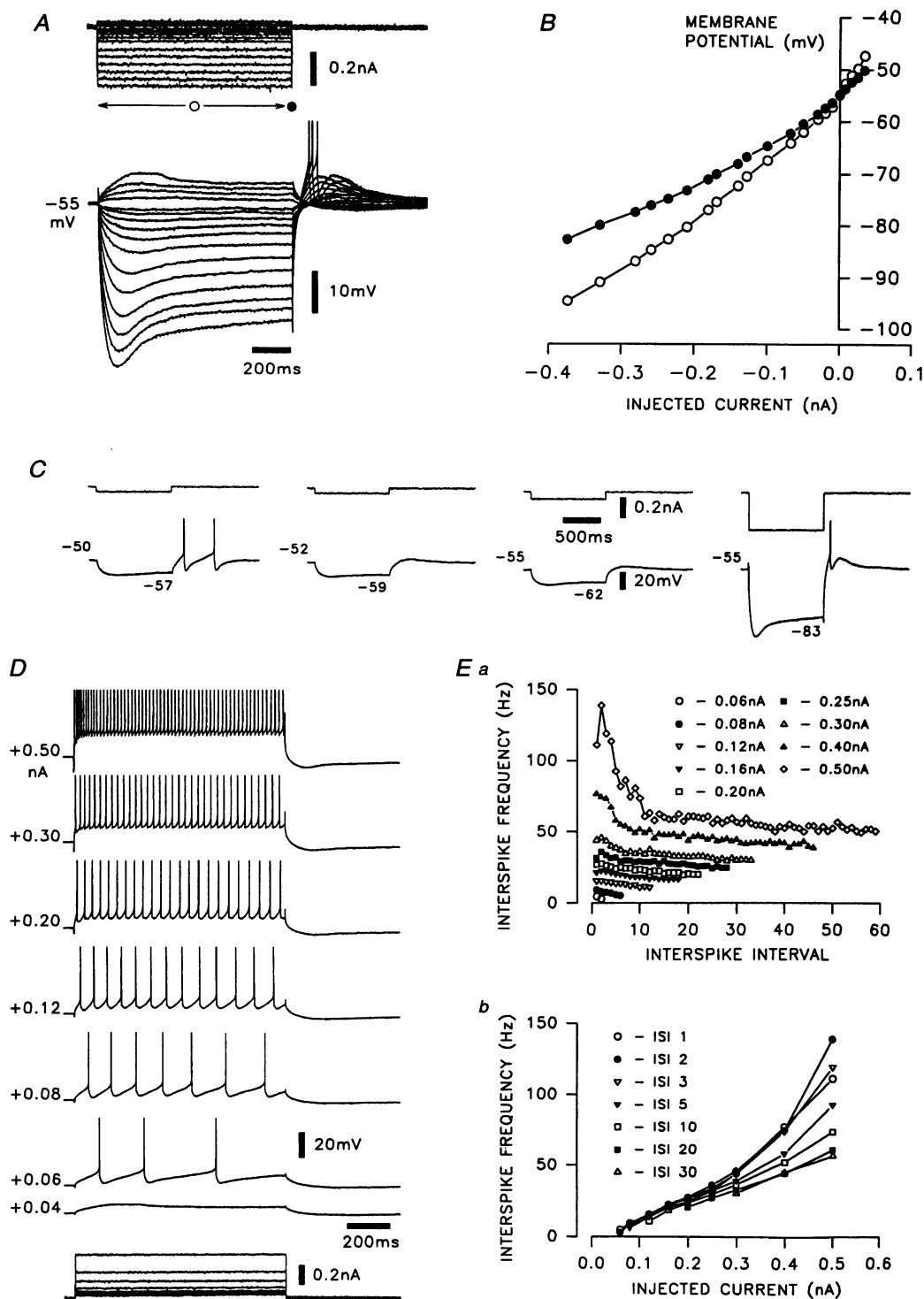
Figure 12. Membrane properties of an interneurone from the cat VB thalamus

A, the overlay of voltage responses (lower traces) of a cat VB interneurone to the current steps (upper traces) illustrated above. *B*, the voltage–current relationships determined at the times indicated by the corresponding symbols in *A* (○, peak; ●, steady state). *C*, the voltage traces illustrate the generation of a low frequency burst of action potentials at the offset of the negative current steps, and its dependence on membrane potential. The membrane potential at the onset and offset of the current pulse are shown to the left of, and below, each trace, respectively. *D*, firing patterns generated in response to positive current steps (lower traces). The amplitude of the action potentials has been truncated for clarity, the injected current is denoted to the left of each trace, and the holding potential is the same as in *A* (−55 mV). *Ea*, the relationship between interspike frequency and interspike interval number for a series of injected currents,

Table 3. Summary of the action potential properties of TC neurones and an interneurone from the cat VB thalamus

		Firing type				
		TC neurones				Interneurone
		Accelerating	Accommodating & intermittent	Burst-suppressed		Accomodating
		(n = 4)	(n = 24)	(n = 13)		(n = 1)
				1st spike	2nd spike	
AP amplitude	(mV)	58·8 ± 4·18	58·9 ± 1·15	49·3 ± 1·85^{d,e}	53·1 ± 1·54^{b,j}	74·0
10–90% rise time	(ms)	0·19 ± 0·014	0·21 ± 0·007	0·28 ± 0·016^{d,f}	0·22 ± 0·009^{j}	0·13
10–90% decay time	(ms)	0·35^{b} (0·28–0·38)	0·47 ± 0·017	0·53 ± 0·042^{e}	0·57 ± 0·055^{a,e,i}	0·26
Half-width	(ms)	0·37 ± 0·016^{c}	0·50 ± 0·017	0·65 ± 0·046^{c,g}	0·61 ± 0·048^{a,e}	0·26
AHP amplitude	(mV)	−13·2 ± 0·98	−13·4 ± 0·38	−15·0 ± 0·76^{a}	−13·4 ± 0·73^{j}	−13·2
AHP time to peak						
Fast	(ms)	1·6 ± 0·29	1·4 ± 0·06	1·6 ± 0·12^{g}	1·6 ± 0·19^{g}	0·74
Slow	(ms)	3·7 ± 0·98^{d}				22·7
AHP decay time	(ms)	31·6 ± 1·81^{d}	16·5 ± 0·87	6·4 ± 0·54^{d,h}	8·4 (4·4–21·3)^{d,g}	275·7
No. per morphological type						
Type I		4	9	5		
Type II		0	8	5		

Action potential and after-hyperpolarization (AHP) amplitude were measured from threshold. After-hyperpolarization time to peak was measured from action potential peak time, and decay time was measured between 10 and 90% of after-hyperpolarization amplitude. For comparisons with accommodating firing type $^{a}P < 0.05$, $^{b}P < 0.01$, $^{c}P < 0.005$ and $^{d}P < 0.001$ (Student's t test or Mann–Whitney U test). For comparisons with accelerating firing type $^{e}P < 0.05$, $^{f}P < 0.01$, $^{g}P < 0.005$ and $^{h}P < 0.001$ (Student's t test or Mann–Whitney U test). For comparison of the second spike with the first spike for burst-suppressed firing type $^{i}P < 0.005$ and $^{j}P < 0.001$ (Student's paired t test or Mann–Whitney U test).

With respect to action potential firing, the accommodating/intermittent and burst-suppressed patterns were fairly equally distributed between the morphological TC neurone types, but the accelerating pattern was only associated with Type I (Table 3). There were no differences in the single action potential properties between morphological type, apart from the amplitude of the action potential after-hyperpolarization, which was smaller for Type I (12·1 ± 0·4 mV) than for Type II (15·1 ± 0·4 mV; $P < 0.05$, Students t test), consistent with the lower outward rectification resistance observed for Type I. Therefore, the only clear distinguishing feature of the membrane properties of morphologically identified TC neurones from the cat VB thalamus was the higher peak input resistance of Type II neurones, and this was reflected by the larger number of these neurones exhibiting delta oscillation (Table 2).

The membrane properties of an interneurone

The morphologically identified interneurone had a resting membrane potential of −55 mV, and a membrane time constant of 61·4 ms, estimated from the voltage responses to −0·01 nA step. The voltage–current relationship for this interneurone exhibited a lack of outward rectification above −60 mV, and only moderate inward rectification below −70 mV (Fig. 12B), so that the peak input resistance between −47 to −57 mV was 205·8 MΩ, and between −80 to −95 mV was 130·6 MΩ. In addition, there was some further time-dependent depolarizing sag of the voltage response (Fig. 12A and C), so that the steady-state input resistance was 56·7 MΩ between −75 and −85 mV (Fig. 12B). Low frequency (3·6 Hz) burst firing was only observed at the offset of negative current steps from holding potentials more positive than −55 mV, while at more negative potentials only a single action potential could be generated (Fig. 12C).

In response to positive current steps, this interneurone was able to generate action potentials when the membrane potential reached a threshold of −42·5 mV, at frequencies of between 5 and 150 Hz, with spike frequency accommodation becoming more prominent as the amplitude of the current step increased (Fig. 12D and Ea). The relationship

showing the marked interspike frequency accommodation at higher injected currents. Eb, the relationship between interspike frequency and injected current for a series of interspike intervals (ISI), showing the non-linear increase in interspike frequency for low interspike interval values with increasing injected current.

between spike frequency and injected current was approximately linear from 0 to 0·25 nA, for all interspike interval frequencies. However, at injected currents of 0·3–0·5 nA, there was a non-linear increase in the interspike frequency for the first to fifth interspike intervals (Fig. 12Eb). The single action potentials of the interneurone were narrower and greater in amplitude than those of TC neurones (Table 3), and had a biphasic after-hyperpolarization (Fig. 11E), with comparable amplitudes to, but much greater times to peak than, those of TC neurones.

DISCUSSION

The main conclusions of this investigation are as follows. (1) The voltage–current relationship for TC neurones from the cat VB thalamus was highly non-linear with a steep region of peak input resistance between −60 and −75 mV, with some neurones also exhibiting a time-dependent increase in voltage response, which accentuated this non-linearity. (2) The action potential characteristics and discharge pattern of these TC neurones varied from an accelerating to a highly accommodating/intermittent or burst-suppressed firing, and were different from those observed in other sensory thalamic nuclei above −60 mV. However, all morphologically identified TC neurones evoked burst firing mediated by a LTCP. (3) Morphologically distinct TC neurones were identified, and differed in their subthreshold membrane properties, with a greater number of the smaller Type II neurones exhibiting delta oscillation, probably due to their higher peak input resistances. (4) The morphologically identified interneurone had a more linear voltage–current relationship, with almost no outward rectification and a smaller inward rectification, and lacked the high frequency action potential firing associated with a LTCP.

The morphology of TC neurones from the cat VB thalamus

The division of TC neurones in the cat VB thalamus into Type I and Type II was based on the qualitative differences in dendritic morphology, and is reflected by the quantitative analysis showing a small but significant difference in the distal part of the dendritic arbor, 160–180 μm from the soma. Since this dendritic region receives the majority of the corticothalamic input (Ralston, 1991; Liu, Honda & Jones, 1995), this difference may be of relevance in thalamo-cortical processing. It has been suggested that the differences in the dendritic architecture of TC neurones are due to scaling (Kniffki, Pawlak & Vahle-Hinz, 1993), and that there are no overall quantitative differences (Havton & Ohara, 1994; Ohara, Ralston & Havton, 1995). However, use of small samples and the intracellular filling of only low threshold mechanoreceptor-activated units may have introduced a bias in these studies. Indeed, while two types of TC neurone have been identified in approximately equal numbers following the retrograde transport of horseradish peroxidase (HRP) injected into the cortex, only four of the

nineteen TC neurones filled following intracellular HRP injection *in vivo* were Type II neurones (Yen *et al.* 1985). Therefore, the approximately equal number of Type I and Type II neurones and the presence of dendritic appendages indicate that ours is a representative sample of the TC neuronal population in the cat VB thalamus, consistent with the observations of Spreafico *et al.* (1983a) and Yen *et al.* (1985).

The subthreshold electrophysiology of TC neurones from cat VB thalamus

In this study the clear defining feature of all the morpho-logically identified TC neurones, but not of the interneurone, was the presence of the LTCP, which has been found to be a characteristic of all TC neurones of the mammalian thalamus studied so far (Jahnsen & Llinás, 1984a; Deschênes *et al.* 1984; Crunelli *et al.* 1987a,b; Hu, 1995; Pape & McCormick, 1995; Williams *et al.* 1996). The voltage–current relationship of these TC neurones, however, are highly non-linear, and the membrane properties in the −60 to −75 mV range of this relationship are not passive, in contrast to previous results in TC neurones of other thalamic nuclei (Bloomfield *et al.* 1987; Crunelli *et al.* 1987a,b; Hu, 1995). It is probable that the properties associated with this region in some TC neurones, whereby the amplitude of voltage responses increases in a time-dependent manner, further accentuates this non-linearity. As demonstrated in the accompanying paper (Williams *et al.* 1997a) the cause of this phenomenon in TC neurones of the cat and rat VB thalamus and dLGN is the expression of the 'window' component of I_T.

The firing patterns of TC neurones from cat VB thalamus

The majority of TC neurones from the cat VB thalamus has markedly different firing properties to those of TC neurones in other sensory thalamic nuclei. Perhaps only those neurones with regular accelerating or moderately accommodating firing patterns could be considered similar to those recorded intracellularly *in vitro* in the cat and rat dLGN (Crunelli *et al.* 1987a,b; McCormick, 1991; Williams *et al.* 1996), and guinea-pig thalamus (Jahnsen & Llinás, 1984a), since these studies revealed remarkable regular firing patterns. Indeed, in TC neurones of the rat VB thalamus, tonic firing is delayed and is much more irregular than that observed in the dLGN (see Fig. 1 in Huguenard & Prince, 1991), indicating that this difference in the firing patterns is a characteristic of the VB thalamus across species. Since the outward rectification observed in TC neurones of the VB thalamus is greater than that reported for other sensory thalamic nuclei *in vitro* (Jahnsen & Llinás, 1984a,b; Crunelli *et al.* 1987a,b; McCormick, 1991; Williams *et al.* 1996), the voltage-dependent conductances active in the range around spike threshold could be determining this difference in firing properties. The more regular firing patterns observed *in vivo* in the cat VB thalamus (Deschênes *et al.* 1984) may result from the neuromodulators released by brainstem afferent activity, since these substances reduce the spike-frequency accom-

modation of action potential firing observed *in vitro* (see McCormick, 1992).

Morphology and electrophysiology: implications for somatosensory physiology

The electrophysiological differences between the morphological types of TC neurone in the cat VB thalamus probably all resulted from the greater peak input resistance of Type II neurones, and led to a greater predisposition to delta oscillation in Type II. During aroused or awake states, when afferent input and membrane conductance are high and membrane potential is depolarized, these differences would have little overall impact on physiological function. Indeed, it is more likely that the functional differences are dependent upon dendritic and synaptic organization, since the difference between transient and sustained responses of TC neurones in the VB thalamus to sensory stimuli (Yen *et al.* 1985) is the strong GABAergic inhibition controlling transient responses (Gottschalt *et al.* 1989). However, during states when afferent input and membrane conductance are low and membrane potential is hyperpolarized such as slow wave sleep (Hirsch, Fourment & Marc, 1982), and during pathological states such as absence epilepsy and the central pain syndromes where burst firing is observed (Jeanmonod, Magnin & Morel 1996), the impact of these differences would be greater. In addition, since the small TC neurones in the VB thalamus project to the superficial layers of the somatosensory cortex (Penny *et al.* 1982; Rausell & Avendaño, 1985), the greater predisposition of the smaller Type II TC neurones to exhibit delta oscillation could be important in the synchronization of thalamocortical networks via these connections either through their intrinsic activity or that driven synaptically.

AVOLI, M. & GLOOR, P. (1982). Role of the thalamus in generalized penicillin epilepsy: observations on decorticate cats. *Experimental Neurology* **77**, 386–402.

BERMAN, A. L. & JONES, E. G. (1982). *The Thalamus and Basal Telencephalon of the Cat. A Cytoarchitectonic Atlas with Stereotaxic Coordinates.* University of Wisconsin Press, Madison.

BLOOMFIELD, S. A., HAMOS, J. E. & SHERMAN, S. M. (1987). Passive cable properties and morphological correlates of neurones in the lateral geniculate nucleus of the cat. *Journal of Physiology* **383**, 653–692.

CRUNELLI, V., KELLY, J. S., LERESCHE, N. & PIRCHIO, M. (1987*a*). The ventral and dorsal lateral geniculate nucleus of the rat: intracellular recordings *in vitro. Journal of Physiology* **384**, 587–601.

CRUNELLI, V., LERESCHE, N. & PARNAVELAS, J. G. (1987*b*). Membrane properties of morphologically identified X and Y cells in the lateral geniculate nucleus of the cat *in vitro. Journal of Physiology* **390**, 243–256.

DESCHÊNES, M., PARADIS, M., ROY, J. P. & STERIADE, M. (1984). Electrophysiology of neurons in lateral thalamic nuclei in cat: resting properties and burst discharges. *Journal of Neurophysiology* **51**, 1196–1219.

GOTTSCHALT, K.-M., VAHLE-HINZ, C. & HICKS, T. P. (1989). Electrophysiological and morphological studies on mechanisms of input–output transformations in single neurones of the somatosensory thalamus. In *Somatosensory integration in the thalamus*, ed. MACCHI, G., RUSTIONI, A. & SPREAFICO, R., pp. 199–216. Elsevier Science Publishers, Amsterdam.

HAVTON, L. A. & OHARA, P. T. (1994). Cell body and dendrites tree size of intracellularly labelled thalamocortical projection neurons in the ventrobasal complex of cat. *Brain Research* **651**, 76–84.

HIRSCH, J. C., FOURMENT, A. & MARC, M. E. (1983). Sleep-related variations of the membrane potential in the lateral geniculate neurons *in vitro. Brain Research* **259**, 308–312.

HU, B. (1995). Cellular basis of temporal synaptic signalling: an *in vitro* electrophysiological study in rat auditory thalamus. *Journal of Physiology* **483**, 167–182.

HUGUENARD, J. R. & PRINCE D. A. (1991). Slow inactivation of a TEA-sensitive K^+ current in acutely isolated rat thalamic relay neurones. *Journal of Neurophysiology* **99**, 1316–1328.

HUGUENARD, J. R. & PRINCE D. A. (1994). Intrathalamic rhythmicity studied *in vitro*: nominal T-current modulation causes robust antioscillatory effects. *Journal of Neuroscience* **14**, 5485–5502.

JAHNSEN, H. & LLINÁS, R. (1984*a*). Electrophysiological properties of guinea-pig thalamic neurones: an *in vitro* study. *Journal of Physiology* **349**, 205–226.

JAHNSEN, H. & LLINÁS, R. (1984*b*). Ionic basis for the electroresponsiveness and oscillatory properties of guinea-pig thalamic neurones *in vitro. Journal of Physiology* **349**, 227–247.

JEANMONOD, D., MAGNIN, M. & MOREL, A. (1996). Low-threshold calcium spike burst in the human thalamus: Common physiopathology for sensory, motor and limbic positive symptoms. *Brain* **119**, 363–375.

JONES, E. G. (1985). *The Thalamus.* Plenum Press, New York.

KNIFFKI, K.-D., PAWLAK, M. & VAHLE-HINZ, C. (1993). Scaling behavior of the dendritic branches of thalamic neurones. *Fractals* **1**, 171–178.

LERESCHE, N., LIGHTOWLER, S., SOLTESZ, I., JASSIK-GERSCHENFELD, D. & CRUNELLI, V. (1991). Low-frequency oscillatory activities intrinsic to rat and cat thalamocortical cell. *Journal of Physiology* **441**, 155–174.

LIU, X.-B., HONDA, C. N. & JONES, E. G. (1995). Distribution of four types of synapse on physiologically identified relay neurons in the ventral posterior thalamic nucleus of the cat. *Journal of Comparative Neurology* **352**, 69–91.

McCORMICK, D. A. (1991). Functional properties of a slowly inactivating potassium current in guinea pig dorsal lateral geniculate relay neurones. *Journal of Neurophysiology* **66**, 1176–1189.

McCORMICK, D. A. (1992). Neurotransmitter action in the thalamus and cerebral cortex. *Journal of Clinical Neurophysiology* **9**, 212–223.

McCORMICK, D. A. & PAPE, H.-C. (1990). Properties of a hyperpolarization-activated cation current and its role in rhythmic oscillation in thalamic relay neurones. *Journal of Physiology* **431**, 291–318.

NOMURA, T., NISHIKAWA, N. & YOKOTA, T. (1992). Intracellular HRP study of nociceptive neurons within the ventrobasal complex of the cat thalamus. *Brain Research* **570**, 323–332.

NUÑEZ, A., AMZICA, F. & STERIADE, M. (1992). Intrinsic and synaptically generated delta (1–4 Hz) rhythms in the dorsal lateral geniculate neurons and their modulation by light-induced fast (30–70 Hz) events. *Neuroscience* **51**, 269–284.

OHARA, P. T., RALSTON, H. J. III & HAVTON, L. A. (1995). Architecture of individual dendrites from intracellularly labelled thalamocortical projection neurons in the ventral posterolateral and ventral posteromedial nuclei of cat. *Journal of Comparative Neurology* **358**, 563–572.

PAPE, H.-C., BUDDE, T. MAGER, R. & KISVARDAY, Z. F. (1994). Prevention of Ca^{2+}-mediated action potentials in GABAergic local circuit neurones of rat thalamus by a transient K^+ current. *Journal of Physiology* **478**, 403–422.

PAPE, H.-C. & McCORMICK, D. A. (1995). Electrophysiological and pharmacological properties of interneurons in the cat dorsal lateral geniculate nucleus. *Neuroscience* **68**, 1105–1125.

PENNY, G. R., ITOH, K. & DIAMOND, I. T. (1982). Cells of different sizes in the ventral nuclei project to different layers of the somatic cortex in the cat. *Brain Research* **242**, 55–65.

PRINCE, D. A. & FARRELL D. (1969). 'Centrencephalic' spike-wave discharges following parenteral penicillin injection in the cat. *Neurology* **19**, 309–310.

RALSTON, H. J. III (1991). Local circuitry of the somatosenory thalamus in the processing of sensory information. *Progress in Brain Research* **87**, 13–28.

RAUSELL, E. & AVENDAÑO, C. (1985). Thalamocortical neurones projecting to superficial and deep layers in parietal, frontal and prefrontal regions in the cat. *Brain Research* **347**, 159–165.

SALT, T. E. (1986). Mediation of thalamic sensory input by both NMDA receptors and non- NMDA receptors. *Nature* **322**, 263–265.

SHOLL, D. A. (1953). Dendritic organization in the neurons of the visual and motor cortices of the cat. *Journal of Anatomy* **87**, 387–406.

SPREAFICO, R., SCHMECHEL, D. E., ELLIS, L. C. JR & RUSTIONI, A. (1983a). Cortical relay neurons and interneurones in the n. ventralis posterolateralis of the cat: a horseradish peroxidase, electron-microscopic, Golgi and immunocytochemical study. *Neuroscience* **9**, 491–509.

SPREAFICO, R., WHITSEL, B. L., RUSTIONI, A. & McKENNA, T. M. (1983b). The organization of nucleus ventralis posterolateralis (VPL) of the cat and its relationship to the forelimb representation in cerebral cortex area SI. In *Somatosensory Integration in the Thalamus*, ed. MACCHI, G., RUSTIONI, A. & SPREAFICO, R., pp. 287–307. Elsevier Science Publishers, Amsterdam.

STERIADE, M. & CONTRERAS, D. (1995). Relations between cortical and thalamic cellular events during transitions from sleep patterns to paroxysmal activity. *Journal of Neuroscience* **15**, 623–642.

STERIADE, M., CURRÓ-DOSSI, R. & CONTRERAS, D. (1993). Electro-physiological properties of intralaminar thalamocortical cells discharging rhythmic (~40 Hz) spike-bursts at ~1000 Hz during waking and rapid eye movement sleep. *Neuroscience* **56**, 1–9.

STERIADE, M., JONES, E. G. & LLINÁS, R. (1985). *Thalamic Oscillations and Signalling.* Plenum Press, New York.

TURNER, J. P., ANDERSON, C. M. & CRUNELLI, V. (1994). Electro-physiological and morphological properties of cat ventrobasal thalamic neurones *in vitro*. *Society for Neuroscience Abstracts* **20**, 55.1.

VERGNES, M., MARESCAUX, C. & DEPAULIS, A. (1990). Mapping of spontaneous spike an wave discharges in Wistar rats with genetic generalized non-convulsive epilepsy. *Brain Research* **593**, 87–91.

WILLIAMS, S. R., TÓTH, T. I., TURNER, J. P., HUGHES, S. W. & CRUNELLI, V. (1997a). The 'window' component of the low threshold Ca^{2+} current produces input signal amplification and bistability in cat and rat thalamocortical neurones. *Journal of Physiology* **505**, 689–705.

WILLIAMS, S. R., TURNER, J. P., ANDERSON, C. M. & CRUNELLI, V. (1996). Electrophysiological and morphological properties of interneurones in the rat dorsal lateral geniculate nucleus *in vitro*. *Journal of Physiology* **490**, 129–147.

WILLIAMS, S. R., TURNER, J. P., HUGHES, S. W. & CRUNELLI, V. (1997b). On the nature of anomalous rectification in thalamocortical neurones of the cat ventrobasal thalamus *in vitro*. *Journal of Physiology* **505**, 727–747.

YEN, C.-T., CONLEY, M. & JONES, E. G. (1985). Morphological and functional types of neurons in cat ventral posterior thalamic nucleus. *Journal of Neuroscience* **5**, 1316–1338.

Acknowledgements

Authors' present addresses

J. P. Turner: Department of Visual Science, Institute of Opthalmology, London EC1V 9EL, UK.

C. M. Anderson: Department of Physiology, University of Birmingham, Birmingham B15 2TL, UK.

S. R. Williams: Reed Neurological Research Center, UCLA School of Medicine, Los Angeles CA 90024, USA.

Author's email address

V. Cruneli: crunelli@cardiff.ac.uk